Effect of misalignment on static and dynamic characteristics of hybrid bearing

Benyebka Bou-Saïd, D. Nicolas

Effects of Misalignment on Static and Dynamic Characteristics of Hybrid Bearings©

B. BOU-SAÏD (Member, STLE)
Institut National des Sciences Appliquees de Lyon
Villeurbanne, Cedex 69621, France
and
D. NICOLAS
Laboratoire de Mecanique des Solides
Pineau 86022, France

The analysis of actual lubrication problems needs to take into account particularities in flow caused by kinematic conditions and contact geometry. For hybrid journal bearings lubricated by low dynamic viscosity fluid, turbulence and pressure drops due to inertia forces in the recess outlets are phenomena which must be taken into account to compute their working characteristics. These bearings serve as both vertical and horizontal shaft guides particularly under low speed conditions. They are used in mechanisms which are highly loaded at start-up and which cannot generate hydrodynamic load-carrying capacities at low speeds. They avoid damage because of their stabilizing effects, but cannot conceptually cope with shaft misalignment. In this paper, the influence of misalignment of geometrical parameters on static and dynamic characteristics of hybrid bearings in laminar and turbulent flow regimes is presented. Experimental results and numerical results obtained with two numerical procedures, i.e., the finite difference method and the finite element method are compared.

KEY WORDS

Hybrid bearings, Misalignment

INTRODUCTION

Hybrid bearings are commonly used as shaft guides, and flow can be turbulent when a low viscosity lubricant is em-

Final manuscript approved February 20, 1991

NOMENCLATURE

$B_{ij} = b_{ij}\, c^3/\mu r^4$	= dimensionless damping coefficients
c	= radial bearing clearance
C_d	= orifice discharge coefficient
d	= orifice diameter
d_m	= projection of axis misalignment
d_{max}	= maximum value of d_m
e_o	= eccentricity at $z = 0$
G_p	= viscosity coefficient due to Poiseuille flow
G_θ	= viscosity coefficient in θ-direction
$G_{\theta c}$	= viscosity coefficient in θ-direction due to Couette flow
G_{zc}	= viscosity coefficient in z-direction due to Couette flow
$H = h/c$	= dimensionless film thickness
$K_{ij} = k_{ij}\, c/(p_o r^2)$	= dimensionless stiffness coefficient
l	= bearing length
M_t	= moment due to hydrodynamic forces
$\vec{n}$	= unit normal outward vector
N	= angular rotating speed (rpm)
$P = (p - p_e)/p_o$	= dimensionless pressure
P_a	= recess pressure
P'_a	= recess pressure at the recess outlet
p_o	= reference pressure
p_e	= external pressure
p_l, p_r	= prescribed left and right pressure
p_s	= supply pressure
$Q = q\mu/c^3\, p_o$	= dimensionless flow in the recess outlet
r	= bearing radius
R_c	= Couette Reynolds number
R_p	= Poiseuille Reynolds number
S	= Bush inside surface
S_a	= recess surface
$\vec{U}$	= fluid velocity vector
U_{mz}	= mean fluid velocity vector component (z-direction)
W	= load-carrying capacity
x	= coordinate
$\mathring{X}$	= velocity component of the shaft center in x-direction
$\mathring{Y}$	= velocity component of the shaft center in y-direction
z	= coordinate
$Z = z/l$	= dimensionless axial coordinate
β	= angle between x-axis and center line
χ	= inertia pressure drop coefficient
$\epsilon_o = e_o/c$	= eccentricity ratio
ϕ	= attitude angle
θ	= circumferential coordinate
ρ	= fluid density
ω	= angular rotating speed (rad/s)
$\Omega = \frac{\mu\omega(r/c)^2}{p_o}$	= dimensionless speed parameter

ployed. These bearings support loads independently of speed, and present stiffness properties which control shaft vibrations. Under ideal operating conditions, the longitudinal axes of both shaft and bush are parallel, although they are displaced eccentrically. However, bearings often operate in a misaligned mode where the shaft and bush axes are inclined to each other. This event, which modifies the static and dynamic characteristics of the bearing, usually occurs in the plane in which the shaft is loaded and is usually due to its flexure. Although solutions are found for aligned hybrid bearings (*1*)–(*4*), and for misaligned journal bearings (*5*), (*6*), none are available for misaligned hybrid bearings.

BASIC EQUATIONS

The theory chosen includes the analysis of bearing turbulent flow performance to take into account possible modifications of flow behavior. Several papers propose representative models. A brief examination of the mechanism shows that between entry and exit, four different flow domains are encountered; the land region, the restrictor region, the recess region and the recess edge region. Each will be considered in turn.

Land Region

The standard thin film theory, or Reynolds equation, cannot correctly model flow variations. Constantinescu (*7*) and Elrod and Ng (*8*) determined the lubricant pressure field in turbulent flow. Starting from these models for an incompressible fluid, the flow is characterized by the following dimensionless equation in the system of axes presented in Fig. 1:

$$\frac{\partial}{\partial \vartheta}\left[H^3 G_\theta \frac{\partial P}{\partial \theta}\right] + \frac{\partial}{\partial Z}\left[H^3 G_z \frac{\partial P}{\partial Z}\right] = \frac{\Omega \partial H}{2\partial \theta} + \mathring{X}\cos\theta + \mathring{Y}\sin\theta \qquad [1]$$

where Ω is the speed parameter which characterizes the hydrodynamic effect compared to the hydrostatic effect and is given by the following expression:

$$\Omega = \mu\,\omega\,(r/c)^2/p_o$$

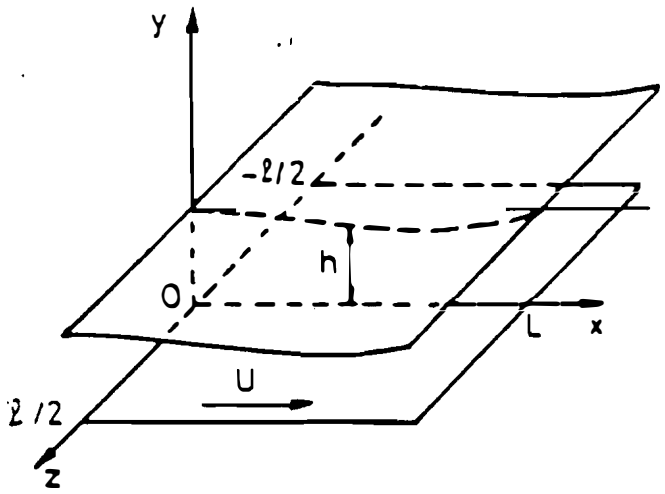

Fig. 1—System of axis.

Equation [1] can study both laminar and turbulent flow. A general domain of study is shown in Fig. 2. Boundary conditions which can appear include imposed pressure on Γ_1, Γ_2, Γ_k and Γ_k, and imposed flow in the recess outlet $\Gamma_i + \Gamma_i + \Gamma_j + \Gamma_j$.

In Eq. [1] the viscosity coefficients G_θ and G_z depend on the Couette and Poiseuille Reynolds numbers (*9*). Constantinescu, et al. (*10*) give the following expressions of these coefficients:

in the laminar regime with $R_p < 1000$ and $R_c < 1000$

$$G_\theta = G_z = 1/12.$$

in the turbulent regime with $R_p > 1000$ and/or $R_c > 1000$

$$G_{\theta c} = 1./(12. + 0.0136\,R_{c^*}^{0.9})$$

$$G_{zc} = 1./(12. + 0.0043\,R_{c^*}^{0.96})$$

with

$$R_c^* = \frac{3}{2}(R_c - 1000)$$

if

$$R_c < 3000$$

and

$$R_c^* = R_c$$

if

$$R_c > 3000$$

with the Couette Reynolds number defined as:

$$R_c = R_{co} \cdot H$$

with

$$R_{co} = \frac{\rho\, r\, \omega\, c}{\mu}$$

and

$$G_p = 6.8 / R_{p^*}^{0.681}$$

with

$$R_p^* = 640. + 1.18\,(R_p - 1000) \text{ if } R_p < 3000$$

$$R_p^* = R_p \text{ if } R_p > 3000$$

and the Poiseuille Reynolds number defined as:

$$R_p = R_{po} \cdot |V_m| \cdot H \quad \text{with } R_{po} = \rho \cdot c^3 \cdot p_o / (\mu^2 \cdot r)$$

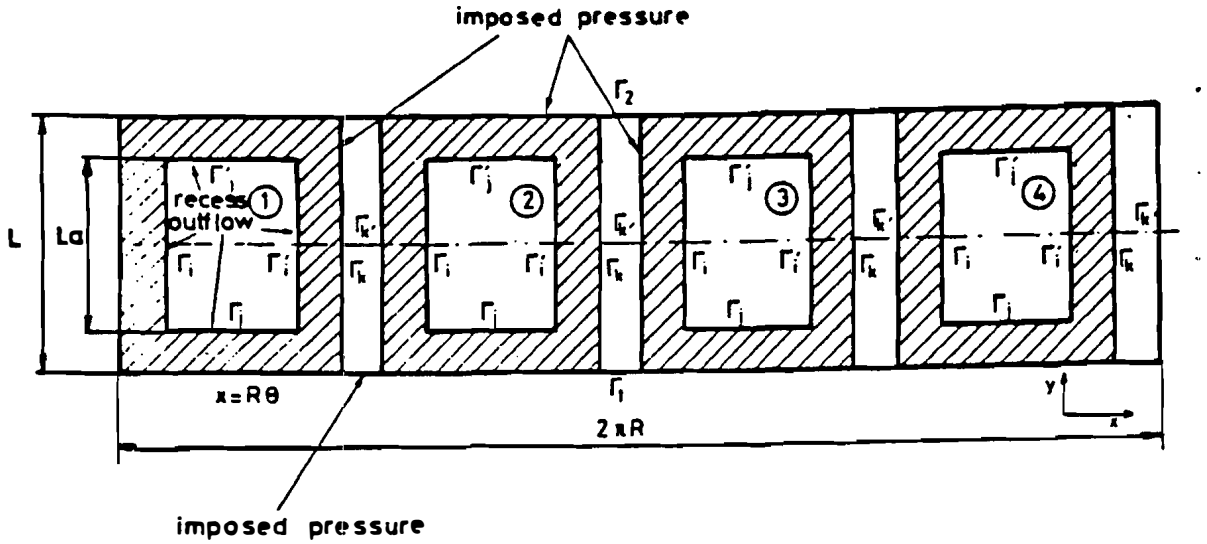

Fig. 2—Domain of resolution.

and

$$|V_m| = H^2 \left[\left(G_\theta \frac{\partial p}{\partial \theta} \right)^2 + \left(G_z \frac{\partial p}{\partial z} \right)^2 \right]^{0.5}$$

Then:

$$G_\theta = \min (G_{\theta c}, G_p)$$

$$G_z = \min (G_{zc}, G_p)$$

Restrictor Region

A hydraulic restriction, which governs bearing stiffness, is mounted between the pump and the recess. The flow through the restriction for an orifice in dimensionless variables is:

$$Q_a = N_q \sqrt{1 - p_a}$$

with

$$N_q = \frac{\mu\, d^2\, C_d\, \pi \sqrt{2}}{4\, c^3 \sqrt{\rho\, p_o}}$$

and

$$p_o = p_s - p_e$$

a reference pressure.

Recess Region

The pressure in the recess is assumed to be constant and equal to p_a. Thus, the pressure generated through speed effects (*11*) is neglected.

Pressure Drop at the Recess Edges

At the recess outlet, the fluid is suddenly accelerated, and inertia effects, which have been studied extensively, induce a pressure drop. The models developed by Constantinescu et al. (*7*) and Chaomleffel (*11*) were used in this study as illustrated in Fig. 3. The dimensionless variables are:

$$P_a - P'_a = N_i\, (\vec{U} \cdot \vec{n})^2 \cdot (1 + X)$$

with

$$N_i = \frac{\rho\, c^4\, p_o}{2\, \mu^2\, r^2}$$

In this expression, N_i characterizes the importance of inertia effects, P_a is the pressure in the outlet section, $\vec{n}$ is the unit normal outward vector, and X is a head loss coefficient which depends on the Reynolds number.

In the axial direction:

$$X = 0.7 \text{ if } R_z < 1000$$

and

$$X = \frac{1.4\ 10^6}{R_z^{2.1}}$$

if

$$R_z > 1000$$

with

$$R_z = \frac{\rho\, h\, u_{mz}}{\mu}$$

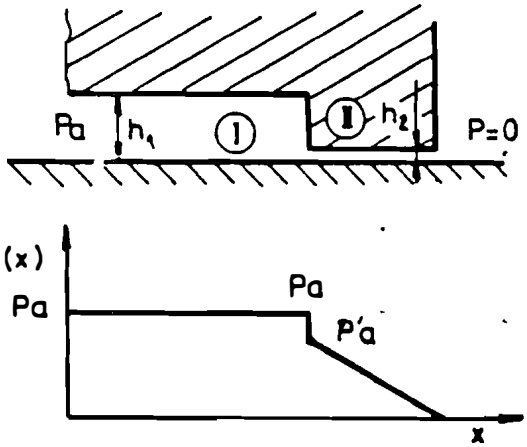

Fig. 3—Pressure drop and pressure distribution.

In the circumferential direction:

$$X = 0.33$$

if

$$R_c < 1000$$

and

$$X = \frac{1.61}{R_c}$$

if

$$R_c > 1000$$

with

$$R_c = \frac{\rho\, r\, \omega\, h}{\mu}$$

The applicable boundary conditions for Eq. [1] are of Dirichlet type, i.e.:

$p\ (z = -1/2) = p_l$ (prescribed left boundary pressure)

$p\ (z = 1/2) = p_r$ (prescribed right boundry pressure)

The pressure at the recess boundary and the outlet flow of the recess, which is equal to the flow crossing the restrictor, are determined by an iterative process.

Film Thickness Representation

The parameters describing the film thickness representation for a misaligned journal are shown in Fig. 4. Here, e_o and Φ_o define the eccentricity vector of the journal center at the midplane of the bearing, d_m is the magnitude of the projection of the journal centerline onto the midplane, d_{max} is the maximum possible value of d_m, and β is the angle between the x axis and the journal centerline projection. Using these parameters, the film thickness equation is given by (*6*):

$$h = c + e_o \cos(\theta - \phi_o) + d_m \frac{z}{l}\cos(\theta - \beta)$$

with

$$d_{max} = 2\,[-e_o\,|\cos(\beta - \phi_o)| + (c^2 - e_o^2 \sin^2(\beta - \phi_o))^{0.5}]$$

Numerical Treatment

The finite difference method and the finite element method were used to solve Eq. [1]. In the finite difference method, Eq. [1] is casted in finite difference form using a grid system (*11*). The algebraic system obtained is solved by the Gauss-Seidel iterative procedure to yield the pressure field. In the finite element procedure, Galerkin's method is used to obtain an integral formulation (*3*). Using a sub-parametric element of approximation leads to a nonlinear system solved by an iterative technique (*3*). In both numerical procedures, the dynamic coefficients are obtained by a finite disturbance technique and the critical mass is calculated using the Routh criteria (*11*).

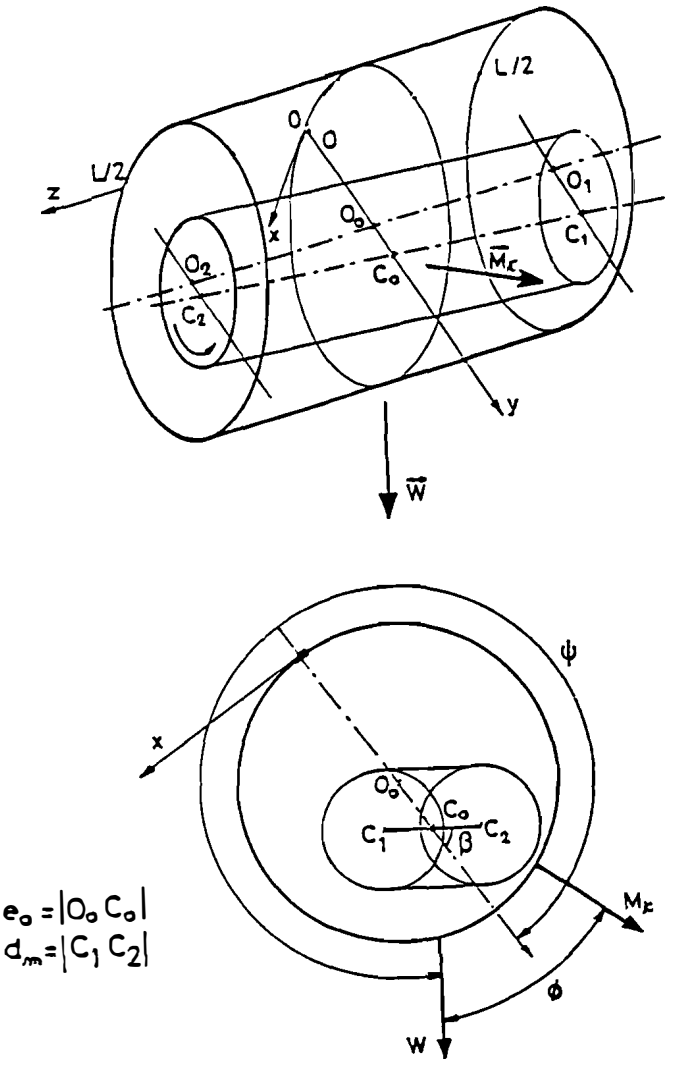

Fig. 4—Misaligned bearing.

TABLE 1—THREE-RECESS HYBRID BEARING

Number of recesses	3
Journal radius	40 mm
Housing length	80 mm
Radial clearance	0.125 mm
Dynamic viscosity	0.001 Pa.s
Fluid density	1000 kg/m^2
Supply pressure	0.4 MPa

Results

Many cases were tested. The first one concerns a three-recess bearing whose characteristics are given in Table 1. The different numerical approaches are compared to those obtained on an experimental apparatus described in detail

Table 2—Four-Recess Hybrid Bearing

	Laminar				Turbulent			
Number of recesses	4				4			
Journal radius (mm)	12.5				125			
Bearing length (mm)	25				250			
Radial clearance (mm)	0.02				0.2			
Dynamic viscosity (Pa.s)	0.00165				0.0002			
Fluid density (kg/m^3)	900				930			
Supply pressure (MPa)	1				1			
Mean Poiseuille number	212				$1.5 \cdot 10^6$			
Inertial parameter	0.34				2380			
Orifice coefficient	0.8				0.8			
Recess width (mm)	10		20		100		200	
Recess length (°)	40		70		40		70	
Sa/S	0.178		0.622		0.178		0.622	
Rotating speed (rpm)	0	12500	0	12500	0	1000	0	1000
Orifice diameter (mm)	0.37	0.2	0.37	0.37	6.7	6.6	8.8	8.7
Mean Couette number	0	178	0	178	0	12150	0	12150
Speed parameter	0	0.84	0	0.84	0	0.008	0	0.008
Orifice parameter	0.74	0.22	0.74	0.74	0.03	0.029	0.051	0.005
Case	1	2	3	4	5	6	7	8

Table 3—Static Characteristics $\varepsilon = 0$

	P_o(10^5Pa)	Q (l/mm)	P_o	Q	
	2.66	34.92	4.87	53.51	FEM
N = 5000 rpm	2.58	36.00	4.62	55.50	FDM
	2.80	34.48	4.80	54.05	Exp.
	3.02	29.89	5.10	51.44	FEM
N = 2000 rpm	2.9	31.70	5.03	52.11	FDM
	3.25	33.89	5.40	48.78	Exp.
P_s	0.4 MPa		0.8 MPa		

elsewhere (*12*). The other cases treated, shown in Table 2, are chosen to study the misalignment effect on static and dynamic bearing characteristics.

Comparison Between Theory and Experiment

Tables 3, 4 and 5 show good agreement between numerical (FDM and FEM) and experimental results for given running conditions in the static case. The divergences noted can be attributed to the calculus assumption. Theoretically, constant pressure in recesses is assumed. Experiments show that this hypothesis is not always valid (*12*). Tale 5 compares the dynamic coefficients obtained by both numerical methods for a supply pressure of 4MPa. The crossed damping coefficients are negligible compared to the direct damping coefficients. The maximum divergence between these results is less than 10 percent.

Misalignment

Tables 6 and 7 consider the vertical shaft case running at $\varepsilon = 0$ and for a β value of zero. Pressure in Recesses 1 and 3, and 2 and 4 are identical because of symmetry. The orifices were sized so that the predicted pressure drop between the supply pressure and the recess pressure would be equal to the drop between the recess and the outside of the bearing for the concentric operation. In the laminar regime, shown in Table 6, the bearing couple depends strongly on both the recess dimension and the rotating speed. For a speed coefficient of 0.84, the hydrodynamic effect is important because of the value of the angle between the moment direction and the x-axis, which is significantly less than 90°. The misalignment increases the recess flow and reduces the recess pressure. Rotating speed has little influ-

TABLE 4—STATIC CHARACTERISTICS $\varepsilon \neq 0$

		EXPERIMENTAL			THEORY (FEM)			THEORY (FDM)		
N (rpm)	ε	ϕ (°)	W (N)	Q (l/mm)	ϕ (°)	W (N)	Q (l/mm)	ϕ (°)	W (N)	Q (l/mm)
2000	0.82	9	763	31.74	8	775	37.9	12.6	671	36.07
5000	0.69	29	763	30.70	20	939	37.2	27.6	757	34.20
8000	0.59	38	763	27.03	29	707	32.1	37.6	755	31.07
2000	0.38	12	356	32.52	10	373	39.3	8.4	328	37.55
5000	0.33	28	356	30.75	20	468	36.5	21	418	34.71
8000	0.27	37	356	27.58	30	421	32.7	32.5	317	31.68

TABLE 5—DYNAMIC CHARACTERISTIC p_s = 0.4 MPa

	FEM			FDM		
	5000 rpm		9000 rpm			
A_{xx}	1.241		1.146			
		1.014			1.01	
A_{xy}	0.364		0.662			
		0.33			0.664	
A_{yx}	−0.325		−0.65			
		−0.33			−0.664	
A_{yy}	1.252		1.144			
		1.14			1.01	
B_{xx}	0.134		0.159			
		1.43			0.149	
B_{xy}	0		0			
B_{yx}	0		0			
B_{yy}	0.126		0.147			
		1.43			0.149	

ence on these characteristics contrary to the recess dimensions. This type of misalignment essentially modifies the stiffness and the damping in the direction of the misalignment plane. For a 0.8 degree of misalignment, a K_{xx} stiffness variation of about 50 percent is observed. Globally, in the turbulent flow regime shown in Table 7, the misalignment has the same effect as in the laminar flow case, but flow variations are lower, due to the existence of turbulence and inertia effects at the recess outlet. Pressure distributions for given running conditions are plotted in Figs. 5 and 6.

CONCLUSION

In solving standard hydrodynamic lubrication problems, computational time is usually lower with the FDM procedure than with the FEM procedure. In hybrid lubrication,

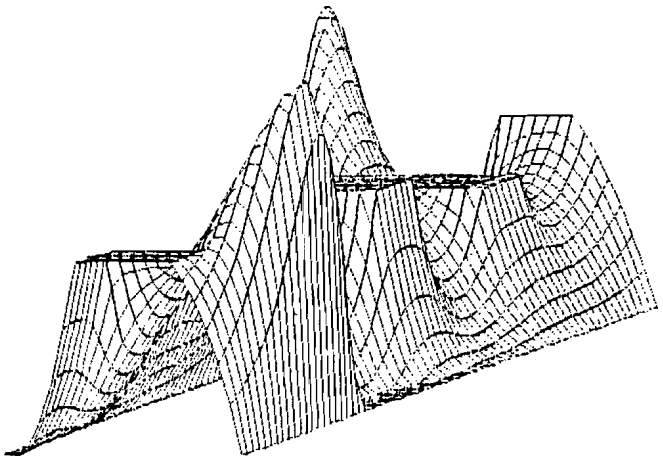

Fig. 5—Pressure field $\varepsilon = 0$ $\beta = 0$ $d_m = 0.8$ $N = 12500$ rpm.

TABLE 6—MISALIGNMENT EFFECT—LAMINAR CASE (N = 0.34)

	CASE	≏	S_a/S	M_t (mN)	(°)	Q%	P_1%	P_2%	K_{xx}%	K_{yy}%	B_{xs}%	B_{yy}%
$\delta = 0.4$	1	0	0.178	0.175	90	2.6	−3.1	−7.4	−6.3	−2	4.2	1.7
	2	0.84	0.178	0.376	27	2.7	−3.2	−7.1	−11.5	1.6	3.3	0.8
	3	0	0.622	0.044	90	5.4	−6.4	−13.5	−21	−4.4	−8.9	−1.9
	4	0.84	0.622	0.057	51.3	4.5	−6.2	−13.2	−21.2	−4	−8.4	−1.5
	CASE	≏	S_a/S	M_t (mN)	(°)	Q%	P_1%	P_2%	K_{xx}%	K_{yy}%	B_{xx}%	B_{yy}%
$\delta = 0.8$	1	0	0.178	0.353	90	8.3	−11.1	−24.7	−17.8	−7.1	38.6	10.1
	2	0.84	0.178	1.02	33.2	7.4	−8.7	−22.1	50	6.7	5	−10.8
	3	0	0.622	0.083	90	14.3	−20.3	−38.3	−52.3	−16.3	−16.8	−4.9
	4	0.84	0.622	0.173	40	13.4	−19.6	−38.2	−46.4	−14.6	−21.3	−6.4

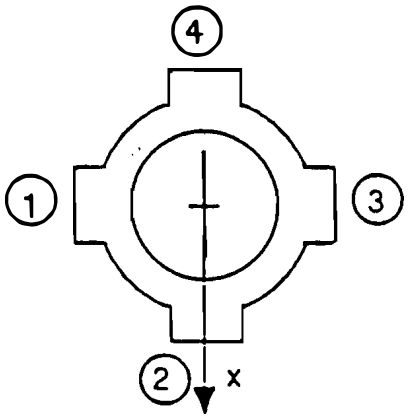

TABLE 7—MISALIGNMENT EFFECT—TURBULENT CASE (N_i = 2380)

	CASE	≏	S_a/S	M_t	ϕ	$Q\%$	$P_1\%$	$P_2\%$	$K_{xx}\%$	$K_{yy}\%$	$B_{xx}\%$	$B_{yy}\%$
δ = 0.4	5	0	0.178	205	90	0.1	−0.3	−0.7	1	1	4	0.8
	6	0.008	0.178	199	79.6	0.3	−0.3	−0.7	1.1	1.1	3.4	2.6
	7	0	0.622	106	90	0.9	−1.2	−1.4	0.3	−1.9	3.8	0.4
	8	0.008	0.622	99.6	86.7	0.6	−1.1	−1.6	−2.9	0	0.8	0.4
δ = 0.8	5	0	0.178	455	90	1.6	−1.1	−3.1	1.6	3.6	22.5	6.7
	6	0.008	0.178	451	79.3	1.1	−1.6	−2.7	13.8	5.5	20.5	8.6
	7	0	0.622	244	90	2.8	−5.2	−6.2	2.7	7.5	25.2	8.9
	8	0.008	0.622	209	86.2	2.9	−4.8	−7.1	−11.8	−1.2	5.8	1.3

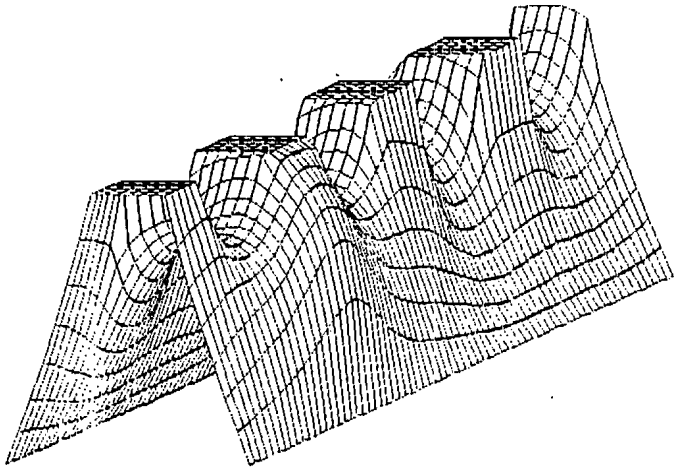

Fig. 6—Pressure field $\varepsilon = 0$ $\beta = 0$ $d_m = 0.8$ $N = 1000$ rpm.

these advantages are reduced. The non-linearities introduced by pressure drops at the recess outlets and the determination of G_θ and G_z coefficients lead to costly iterative processes. Misalignment induces a flow increase which causes a recess pressure drop. This effect is such that the recess dimension is important. In the non-laminar regime, the existence of turbulent flow associated with inertia effects at the recess outlet reduces the misalignment influence. The misalignment can strongly modify the dynamic coefficients, and these variations depend on bearing geometry and running conditions. In the hydrostatic regime, small values of crossed stiffness and damping coefficients are found. In all the cases tested, no unstable variations of the critical mass were detected.

REFERENCES

(1) Rhode, S. M. and Ezzat, H. A., "On the Dynamic Behavior of Hybrid Journal Bearings," *ASME Trans. Jour. of Trib.*, **98**, 1, pp 90–94 (1976).

(2) Heller, S. and Shapiro, W., "A Numerical Solution for the Incompressible Hybrid Journal Bearing with Cavitation," *ASME Trans. Jour. of Lubr. Tech.*, pp 508–515(1969).

(3) Bou-Said, B. and Chaomleffel, J. P., "Hybrid Journal Bearing: Theoretical and Experimental Results," *Jour. of Trib.*, **111**, 2, pp 265–269 (1989).

(4) Degueurce, B. and Nicolas, D., "Turbulent Externally Pressurized Bearings—Analytical and Experimental Results," *Proc. for the 2nd Leeds-Lyon Symp.—Superlaminar Flow in Bearings*, pp 228–232 (1975).

(5) Singh, D. V. and Sinhasan, R., "Performance Characteristics of an Ungrooved Big End Bearing with Misalignment," *Trib. Trans.*, **32**, 2, pp 234–238 (1989).

(6) Bou-Said, B. and Chaomleffel, J. P., "Influence du Mesalignement sur les Caracteristiques Dynamiques des Paliers à Lobes," *Jour. de Mecanique Theorique et Appliquee*, **6**, 3, pp 409–421 (1987).

(7) Constantinescu, V. N., Galetuse, S. and Kennedy, F., "On the Comparison between Lubrication Theory, Including Turbulence and Inertia Forces, and Some Existing Experimental Data," *ASME Trans. Jour. of Lubr. Tech.*, pp 439–449 (1976).

(8) Elrod, H. G. and Ng, C. W., "A Theory of Turbulent Fluid Film and its Application to Bearings," *ASME Trans. Jour. of Lubr. Tech. Series F*, **89**, 3, pp 346–362 (1967).

(9) Constantinescu, V. N., "On Turbulent Lubrication," *Proc. of the Inst. of Mech. Eng.*, **173**, 38, pp 881–900 (1959).

(10) Constantinescu, V. N., Pan, C. H. T., Smalley, A. J. and Vohr, J. A., "Lubrication Phenomena in a Film of Low Kinematic Viscosity," *Rev. Roum. Sc. Tech. Mech. Appl.*, **15**, 2, pp 479–502 (1970).

(11) Chaomleffel, J. P., "Influence des Forces d'Inertie en Lubrification Hybride," Ph.D. thesis, National Institute of Applied Science, Lyon, France (1983).

(12) Chaomleffel, J. P. and Nicolas, D., "Experimental Investigation of Hybrid Journal Bearings," *Trib. Intl.*, **19**, 5, pp 253–259 (1986).